



Dynamic presbyopia correction in the macular field of view by using a liquid crystal lens

LOUIS BÉGEL¹ AND TIGRAN GALSTIAN^{1,2,3,*}

¹*Center for Optics, Photonics and Laser, Department of Physics, Engineering Physics and Optics, Université Laval, Pavillon d'Optique-Photonique, 2375 Rue de la Terrasse, Quebec G1V 0A6, Canada*

²*TLCL and LensVector inc., 2375 Rue de la Terrasse, Quebec G1V 0A6, Canada*

³*PATQER Photonique inc., 2375 Rue de la Terrasse, Quebec G1V 0A6, Canada*

*tigran.galstian@phy.ulaval.ca

Abstract: A large aperture matrix of tunable liquid crystal lenses (MTLCL) is used for dynamic presbyopia correction. The special electrode design and driving method allow the activation of local lenses at arbitrary lateral positions of the MTLCL. First, the study of tunable wavefronts, which can be generated by such a device, is presented. Then, the image quality at different viewing angles and distances is quantified. A driving algorithm has also been developed to increase the speed of focusing. It is shown that this device may provide continuous focus tunability (from 0 to 2.5 diopters), react within 0.5 s, operate with relatively low voltages (<5 V), and enable diffraction-limited on-axis aberrations. Finally, the results of a comprehensive evaluation of its performance with human subjects are reported, comparing the visual acuity (VA) achieved by using the approach proposed in this project against the natural human VA for objects in the near field.

© 2025 Optica Publishing Group under the terms of the [Optica Open Access Publishing Agreement](#)

1. Introduction

As the global population ages, a significant challenge in ophthalmic health emerges: presbyopia. This age-related condition, affecting the eye's ability to focus on nearby objects, is a consequence of the loss of the capability to dynamically deform the crystalline lens (hardening, loss of strength or elasticity, etc. [1,2]), typically occurring in individuals around their mid 40s to 50s [3]. Presbyopia is more than a mere inconvenience; it represents a profound shift in the individual's visual experience, impacting daily activities and overall quality of life. Currently, over a billion people worldwide grapple with presbyopia [4] and this number is expected to rise with the aging demographic. In all attempts to address this problem, the ability to seamlessly switch between near and far vision correction is a critical issue, addressing the need for a more natural and wide-ranging visual experience. Traditional corrective approaches, such as single vision, monovision, bifocal, and progressive lenses [5], offer partial solutions but are fraught with limitations. For example, while some recent bifocals are built to reduce image jumps, traditional fixed discrete optical power (OP) zones can cause such jumps and a reduced natural field of view (FoV). Progressive lenses, despite their seamless power progression in vertical direction, induce peripheral astigmatism [6] and often require head movement for clear near vision. These inconveniences and the physical discomfort associated with currently used corrective methods, underscore the need for more innovative and adaptable solutions.

An interesting solution for presbyopia would involve restoring the flexibility of the crystalline lens or employing a type of focus-adjustable lens. Currently, surgical techniques are being researched that focus on either reducing the stiffness of the crystalline lens or replacing it with a flexible intraocular lens [7]. However, these surgical methods come with the inherent risks of invasive procedures and are predominantly in the experimental phase, with long-term efficiency and reliability yet to be established. A significant limitation of the methods described above is that they offer only a fragmented or distorted correction of vision, which is not natural. For a

true restoration of normal vision, active correction of accommodation may be necessary. This means that the correction must be responsive to the distance of the object being observed, without compromising the visual field or requiring adjustments in the viewing angle. To achieve this, the focus-tunable element could also be placed outside the eye. A variable OP change of 3.0 Diopters (D, the inverse of focal distance in meters) is needed here [7]. Efforts to create such variable-focus eyeglasses led to several interesting solutions, such as sliding Alvarez lenses [8] or liquid filled lenses [9]. Subsequent enhancements in the actuation mechanism of these lenses have been proposed [10,11].

To avoid mechanical movements or deformations, variable-focus lenses can also be made by using other technologies, e.g., liquid crystal (LC) lenses [12,13], deployed as contact lenses [14] or intraocular lenses [15]. However, for wide-aperture optical systems (such as human vision that requires large-diameter optics) LC lenses face their own drawbacks. Namely, if the aperture size of an LC lens increases while the LC layer's thickness remains constant, the OP decreases according to a quadratic relationship. Consequently, active research is being conducted to develop LC Fresnel lenses [16–20]. However, the manufacturing of LC variable-focus lenses with apertures in the range of 25 mm - 50 mm (for eyeglasses) remains a challenge. Fresnel zones' boundary scattering, diffraction effects between electrodes, capacitive effects, etc. remain significant limitations [12,13,21,22].

At the same time, it is well known that the human vision is angle dependent, with a small retinal area that provides the sharpest VA needed for detailed tasks, such as reading. It provides images focused at different distances along the optical axis and is, therefore, a matter of central “foveal” or “macular” viewing. Therefore, a new electrode structure has recently been developed with serpentine electrodes in the LC cell [23–25] capable of locally activating lenses in a wide FoV (in arbitrary lateral positions) with variable diameters and focal lengths.

In this work, our primary aim is to conduct an evaluation of the potential of using such focus-tunable eyeglasses (based on this new approach) as a method of correction for presbyopia by correcting exclusively the foveal and macular FoV, without noticeably altering the rest of the FoV. Thus, preliminary characterization work is presented, describing the wavefront, OP, aberrations and speed of the lens. Finally, the results of human vision correction tests (performed on 7 patients) are presented.

1.1. Design and operating principle of the lens

The operating principle of the proposed matrix of tunable LC lenses (MTLCL) has already been described in detail in [24,25]. Its schematic diagram is shown in Fig. 1(c). The structure consists of a planar LC cell formed by two transparent substrates (usually glass, but can also be plastic) with transparent conductive coatings (on their inner surfaces) made of a thin layer (approximately 30 nm thick) of indium tin oxide (ITO). Using the photolithography process, serpentine ITO electrodes with a width of 35 μm and a gap of 5 μm are patterned orthogonally on both substrates (see Fig. 1(a), (b)). For the moment, this patterning creates a very weak diffraction from etched edges of the ITO. However, this is not noticeable and can be mitigated later by using ITO with index matched layers. While the number of control electrodes (external contact points) can be varied, the current design features 40 control contacts per substrate, with a total active area of 25 mm \times 25 mm. A resistance of 1 M Ω was measured between neighboring contact electrodes spaced 0.64 mm apart [24]. These serpentine ITO surfaces are coated (on both the upper and lower substrates) with a parallel-alignment polyimide film (from Nissan) and uniformly rubbed. These substrates are then aligned parallel to each other to form a sandwich with a gap that is maintained by polymer ball spacers (with an average diameter of 60 μm). The cell is filled with a nematic LC (NLC) material, MLC-2048 (from Merck, Germany), [26,27], by capillary action. This material was selected, first of all, for its well-documented dielectric and viscoelastic properties (see hereafter).

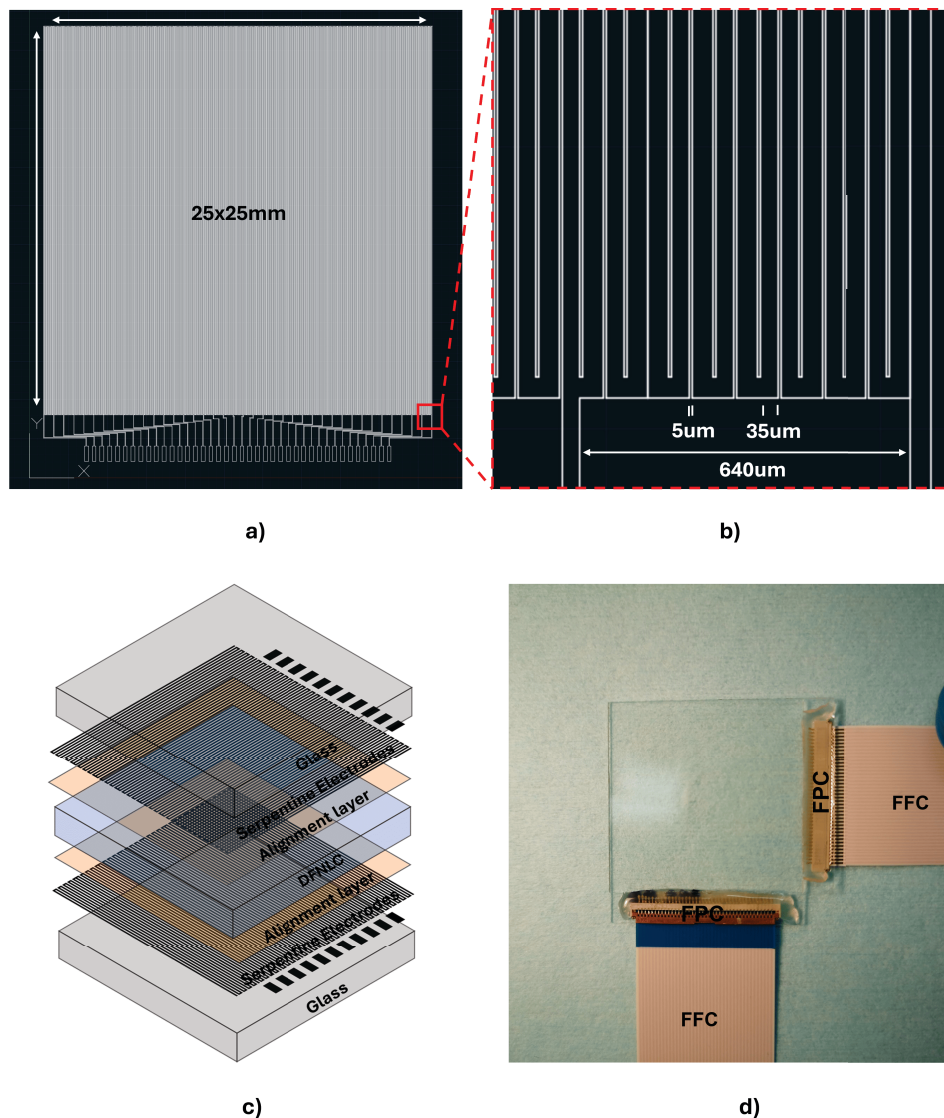


Fig. 1. a) Schematic top view of transparent electrodes of the lens. b) Zoom on the corner of the patterned electrodes and c) Schematic 3D view of the lens. External contact electrodes (dark rectangles) are arranged at a constant distance. d) Top photography of the lens with flat printed connectors (FPC) and flat flexible cables (FFC).

In order to generate four control electrical signals (described in [24,28]), a driving module has been designed and built. It consists of a custom electrical phase shift waveform generator. A micro controller generates two high-frequency waves F_1 and F_2 (here, with the same specific frequency values F but with 90° phase shift Φ), as well as one low-frequency f signal (typically 20 Hz) as an offset component. Buffer/inverter pairs create balanced positive(P)/negative(N) versions of these signals F_{1P}/F_{1N} ($\Phi 0^\circ/180^\circ$), F_{2P}/F_{2N} ($\Phi 90^\circ/270^\circ$), and f_P/f_N ($\Phi 0^\circ/180^\circ$). These 6 signals are then amplified up to desired values of U for high frequency signals and U_{off} for low frequency (offset) signals to produce balanced \sin waves. These amplified signals are combined (as detailed in [24]) to produce 4 signals, applied to 4, dynamically changeable, peripheral contacts A, B,

C and D, as follows : A ($F_{1P} + f_P$), B($F_{1N} + f_P$), C($F_{2P} + f_N$) and D($F_{2N} + f_N$). Finally, 160 1/8 multiplexers are used to generate the drive outputs. The multiplexers can select an open-circuit (floating), one of the A/B/C/D signals, or the ground to be applied to MTLCL's electrodes.

The authors have previously demonstrated the capability of this device to locally create and adjust (through a large aperture) a variable focal length lens without noticeably disturbing the rest of the FoV [24]. That device was using a polarizer. Here (in the last section), results are presented with an electrically tunable polarizer-free MTLCL (built by using two LC layers, see hereafter), which is more appropriate for ophthalmic applications. Indeed, due to the anisotropic properties of the NLCs used here, the lens with a single NLC cell (or so-called, "half-lens") exhibits polarization-dependence (it is focusing only the extraordinary polarization component of light). For ophthalmic applications, it is crucial that these lenses operate with unpolarized light. To achieve this, two identical NLC layers must be assembled together [29] (what is called here a "full-lens") with their ground state molecules being oriented in orthogonal planes.

Such a lens is schematically demonstrated in Fig. 2. Small orange ellipses schematically represent NLC molecules. The longer the ellipse, the larger is its projection on the drawing plane. Thus, in the ground state, Fig. 2(a), molecules of the first sandwich (on the left) are perpendicular to the drawing plane, while molecules of the second sandwich are in that plane (oriented vertically). For the specific choice of positions of target objects (letters E and F), they appear blurry on the plane of the retina if the lens is in the ground state, Fig. 2(b). Figure 2(c) demonstrates the case when an appropriate local lens is activated to focus the letter E. In this case, the letter F (which is out of the region of interest, RoI) appears blurry on the retina. In contrast, Fig. 2(d) demonstrates the case when the neighboring local lens is activated to focus the letter F. In this case, the letter E (which is now out of the RoI) appears blurry on the retina.

The optical performance of half and full lenses are very similar. For example, the maximum achievable range of OP is still the same, defined by the birefringence of the NLC material, its thickness and the local lens diameter (often called clear aperture, CA), [24], see, Eq. (2). The main question here is how to insure that the two half lenses (NLC layers) of the full lens focus at the same focal plane to avoid image degradation. Indeed, two orthogonal polarized components may be focused at different distances, generating thus, so-called "polarization aberrations" [30]. However, using relatively thin substrates (particularly internal ones, see Fig. 2) allows achieving very good results [15,31].

The choice of the working CA of the local lens also is crucial for ophthalmic applications. In human vision, the VA decreases rapidly from the fovea to the periphery due to the decrease of the cone photoreceptor density [32]. At the center of the fovea (within approximately 2°), VA is maximal, associated with what is called "Normal" or 20/20 (Snellen ratio) vision that corresponds to a minimum angle of resolution (MAR) of 1.0 minute of arc, i.e., when the smallest recognizable letter subtends an angular height of 5 minutes from the eye and each element of the letter subtends 1 minute. In comparison, a VA of 0.5, also expressed as 20/40 in Snellen terms, corresponds to a MAR of 2.0 arcminutes [33]. Moving towards the periphery of the macula beyond approximately 5° where the density of rods exceeds the density of cones [34,35], VA drops approximately 70% and beyond a 60° deviation from the fovea, VA approaches zero [36]. Due to this decrease beyond the foveal area, we can limit the CA of the local lens while moving it across the entire lens matrix. Obviously, an eye tracking capability must be provided with such a lens to follow the eye movements (see hereafter).

Correspondingly, the CA of our local lens was optimized to cover the total FoV of the macula. Aligning the optical axis to the center of the macula, its FoV, seen from the air, can be approximated as [37]:

$$FoV = 2\sin^{-1} \left(\frac{L_m n_{avg}}{\sqrt{L_m^2 + 4L_e^2}} \right) \quad (1)$$

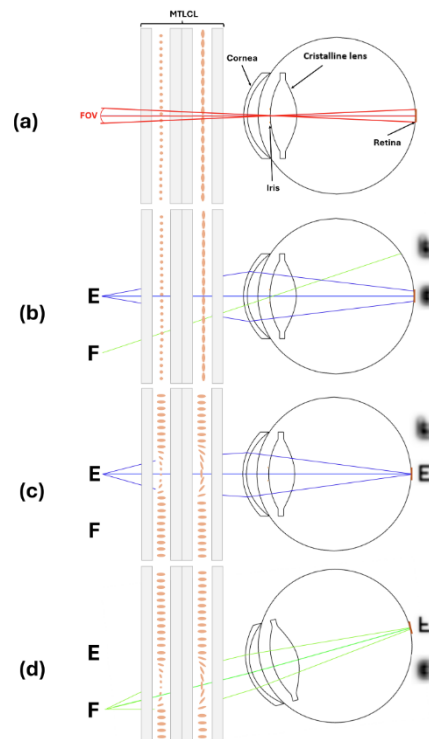


Fig. 2. Schematic representation of the proposed MTLCL with two (cross-oriented) LC layers (sandwiched between two flat substrates and laminated together) with dynamically changing positions of local lenses following the region of interest (RoI) for a human eye. The orange ellipses represent molecules. a) The limited field of view (FoV) focusing on the retina, with the tunable lens size (local CA) necessary to adjust the focus on the retina. b) The focal shift on the retina with a presbyopia eye. c) Local lens activated in the RoI to bring in focus the letter E, while keeping uniform the periphery (under the red colored electrodes). d) The same as above but for the letter F.

where L_m is the size of the macula and n_{avg} is the average refractive index of the eye. Given $L_m = 5.5$ mm and $n_{avg} = 1.369$ [38], FoV is around 17° - 18° . Usually, eye glasses are placed at $D \approx 16$ mm from the eye, and the MTLCL is supposed to be attached to them. Thus, to adequately cover the macular FoV, the CA of the local lens on the MTLCL must have a diameter greater than $CA > 5.1$ mm.

2. Experimental results

2.1. Image quality tests

The characterization of the lens' performance began by using a Shack-Hartmann wavefront sensor (SHWFS). It allows the measurement of key optical properties, including the focal length and aberrations under various applied voltages. A continuously working (CW) He-Ne laser (operating at 632.8 nm) provided the probe beam at normal incidence on the lens. The SHWFS captured the probe's wavefront at the output of the tunable lens (a fixed relay lens was used to create the image of this output on the microlens array of the SHWFS).

Initial measurements were performed with zero applied voltage for the calibration of the SHWFS, followed by incremental voltage applications with wavefront recordings at each step. The results obtained (Fig. 3) demonstrate the relationship between the applied voltage and the

focal length of the lens, as well as the corresponding values of astigmatism, coma, and spherical aberration. Usually, root mean square (RMS) aberrations are used to assess the quality of the lens by quantifying how much the lens distorts the wavefront of light (with respect to the desired one, e.g., spherical) passing through it. This is necessary for applications, such as ophthalmic lenses, where minimizing aberrations is essential for clear vision correction in real-time. RMS aberrations at the level of $\lambda/4$ are commonly cited as an acceptance threshold [39,40]. An optical system with RMS wavefront error less than $\lambda/4$ is generally considered to be performing at a level where diffraction effects dominate over aberrations. This is often used as a practical criterion for good optical quality.

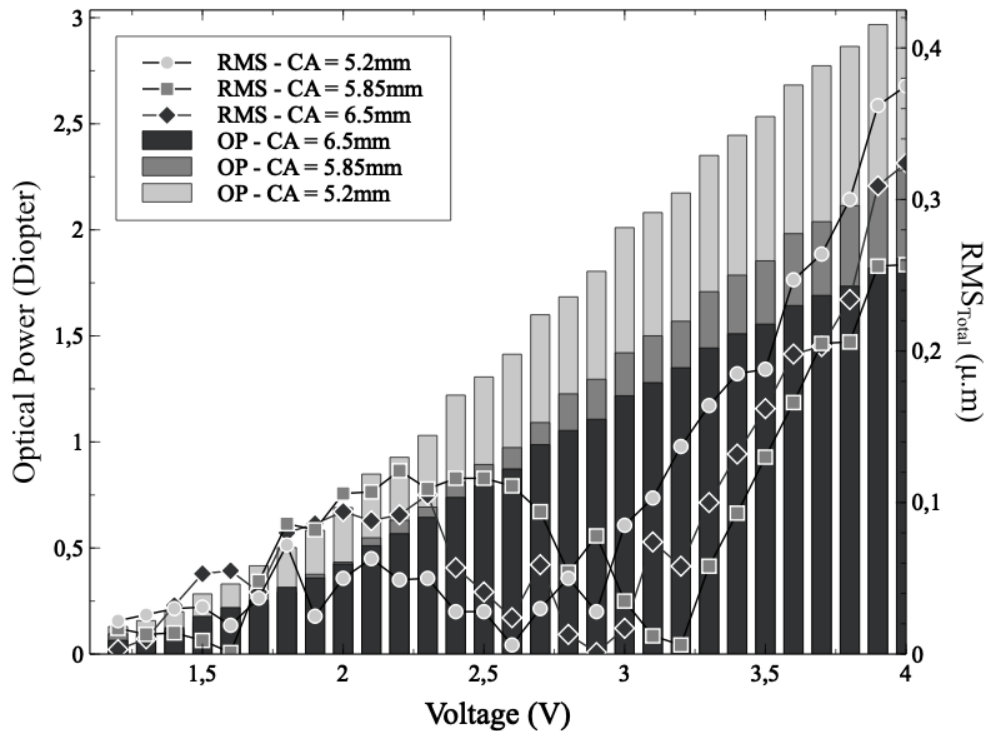


Fig. 3. Excitation dependencies of RMS aberrations and OP values for various sizes of the clear aperture of the local lens.

Figure 3 shows results obtained for CA values larger than required (5.2 mm, 5.85 mm and 6.5 mm). As can be seen, 2.5 D (diopter correction to be able to correct 85% of presbyopic eyes [7]) can be reached while still keeping optical aberrations at a rather low level. All voltages hereafter are presented in their RMS values. It is worth mentioning that the MTLCL acts like a capacitive charge. Its electrical current and power consumption are very low [15] and there is no noticeable ohmic heating. Thus, the MTLCL shows a good potential for ophthalmic applications, where a specific ROI may be observed with higher quality within the entire FoV of the local lens.

Figure 4 is qualitatively demonstrating how the local lens may bring into focus various ROIs (a-in the center and b-shifted towards the top left) of a target image consisting of a 2D array of small white squares. The dashed white square demonstrates the total MTLCL area, FFC 1/2/3 and 4 correspond to the flat flexible cable positions, which were activated to address electrodes to create the local lens in the Fig. 4(a).

Then, the lens was used to perform more quantitative image characterizations. To this end, six targets (binary black and white patterns) of multiple lines pair sizes were placed simultaneously

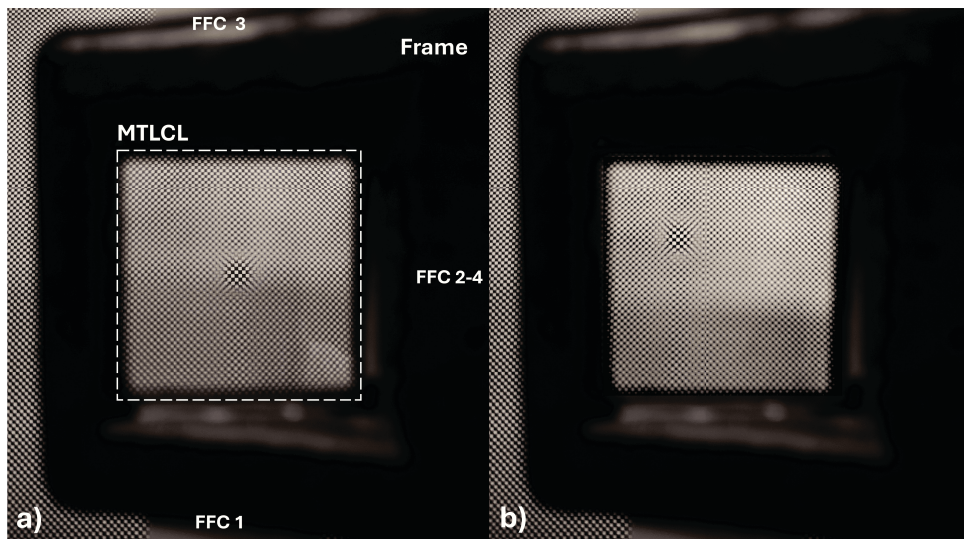


Fig. 4. Comparative images of a target object (2D array of white squares) formed with the use of the MTLCL for different regions of interest, a) in the center and b) shifted to the top left. Dashed square corresponds to the MTLCL area. FFC1/2/3 and 4 correspond to the flat flexible cable positions activated to create the lens in a).

at 100 cm, 60 cm, and 35 cm from the MTLCL (which was placed in front of a raspberry pi HQ Camera, coupled with a 16 mm objective) at different viewing angles (to ensure that all these targets are within the total FoV of the camera), Fig. 5(a). The camera was adjusted in order to mimic (approximately) the human eyes with presbyopia. Namely, for each distance, the smallest feature (printed in our experimental charts) corresponds to 20/20 vision, that is, if we can differentiate the minimal feature (a black bar) then it corresponds to 1 arcmin. When the OP of the MTLCL was 0 D, the target at 100 cm (center/top) was in focus and thus could be recorded with good quality, Fig. 5(a). At the same time, all other targets are out of focus. When the OP of the LC lens was 1.5 D (CA = 5.2 mm), target 2 (placed at 60 cm on the left) appeared in focus, Fig. 5(c). When the OP of the local LC lens was tuned to 2.5 D, then target 1 (placed at 35 cm in the center) became clear, Fig. 5(b). These targets allowed us to extract the quantitative information (modulation transfer function or MTF) about the contrast enhancement with corresponding focus correction (shown in Fig. 5).

As can be seen, noticeable improvement is observed for the MTF values when local lenses are activated. For example, at 0.8 cycles/mm, the growth of the MTF is by an approximate factor of 2 for the target 1, while this factor is 4.4 for the target 2. On average, at this point, they are only at 24% below the diffraction limit. This is a rather considerable improvement. It is important to mention that the contrast degrades at the level of the smallest features (corresponding to 1 arcmin), but it is still possible to differentiate the two targets. In any case, it is also important to keep in mind that the analogy with human vision is not perfect here since there are other parameters affecting this performance (such as pixel characteristics of the camera, etc.).

While black and white images were used in this work, the image recording was performed by using a color (RGB) camera. As one can see, the edges of black and white zones remain very clear (without coloration) when the image is brought into focus. This shows that the chromatic aberrations are rather small at all spatial frequencies (averaged in the visible spectrum of the camera). In addition, the same lens was used in the past to record images of colored objects

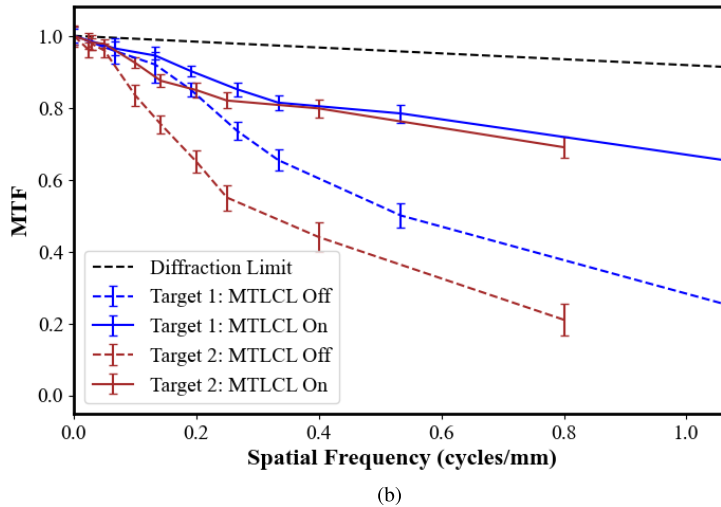
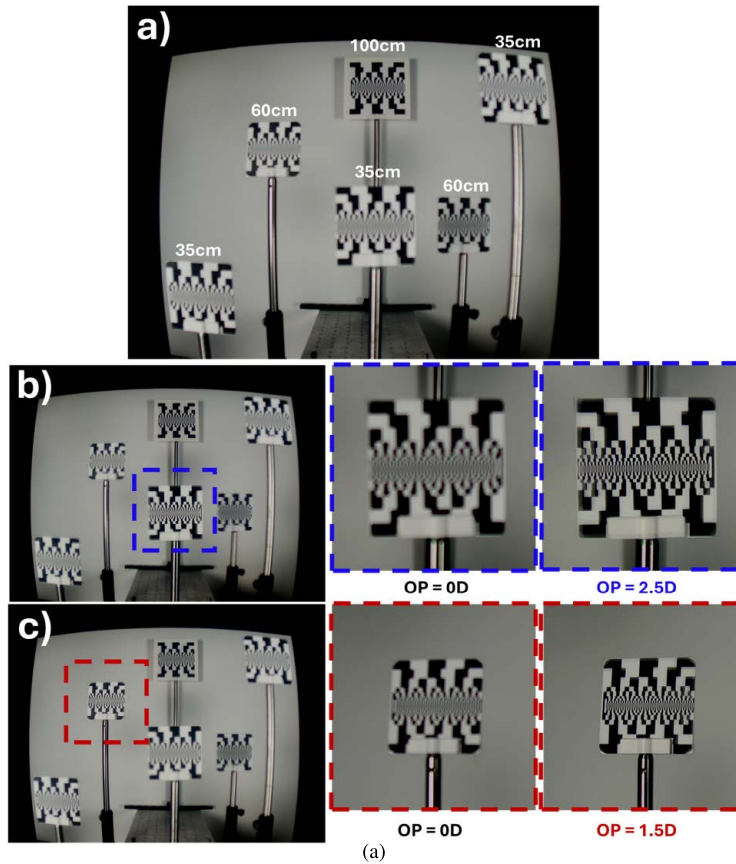


Fig. 5. (a) The experimental scene with 6 objects, placed at various positions (at 100, 60 and 35 cm from our lens) and at various angles. Demonstrated examples : a(b) - a local lens is activated (with $OP=2.5$ D) to focus on the target 1 (placed at 35 cm in the center), a(c) - The next local lens is activated (with $OP=1.5$ D) to focus on the target 2 (placed at 60 cm on the left). (b) Modulation Transfer Function (MTF) calculated for two different targets.

(described in the Fig.10 of [24]), and results reported there also confirm that chromatic aberrations are low.

2.2. Transition speed measurements and optimization

One of the fundamental problems in the development of electrically controlled NLC lenses is their slow response time. For vision corrections, the accommodation time of the eye typically ranges from 0.3 s to 0.6 s in healthy adults [41]. In addition, the MTLCL's operation must comply with a real-time eye-tracking system. Thus, the entire system must adapt the MTLCL's OP and lateral position within these time scales to maintain clear vision across different viewing distances.

Also, the NLC layer of the MTLCL needs to be relatively thick since the lens is operating in the refractive gradient index (GRIN) mode [42]. This is necessary to provide enough optical path difference $OPD=\delta nd$ (where d is NLC thickness and δn is the refractive index modulation depth that is limited by the optical birefringence Δn of the NLC) and corresponding range of focus changes. Indeed, the maximum achievable OP of a GRIN lens may be approximated as

$$OP \approx \frac{2 \times OPD}{(CA/2)^2} \quad (2)$$

Thus, the increase of d may help. However, by increasing d , we increase the time needed for the change of average orientation of the long molecular axis of the NLC (often called *director* [43]). Thus, the natural relaxation time τ_{off} (when the electrical voltage is simply switched off after some degree of excitation and NLC molecules orient back to the original state that is defined by the surface alignment in the cell) is described [44] by the following equation:

$$\tau_{off} \approx \frac{\gamma_1 d^2}{\pi^2 K} \quad (3)$$

where γ_1 and K are the rotational viscosity and elastic constants of the NLC, respectively. More detailed analyses should also take into account the fact that the excitation process may involve different types of director deformations. In this case, we should also consider different elastic constants. However, very often, a “one-constant” approximation works very well.

As one can see from Eq. (3), the natural relaxation time τ_{off} (sometime also called turn-off time) depends only on material characteristics (γ_1/K) and the thickness d of the NLC. However, the excitation (or turn-on) time can be controlled also by the value of the applied (excitation) voltage U :

$$\tau_{on} \approx \frac{\tau_{off}}{((U/U_{th})^2 - 1)} \quad (4)$$

where U_{th} is the threshold voltage (typically at the order of 1V) of the director's reorientation [45]. It is also worth mentioning that, in so-called “modal-control” tunable lens designs (which is also the case here), the spatial distribution of electrical potential (and thus the local value of U) depends upon the excitation frequency due to the effective distributed RC circuit defined by the geometry (the structure) of the lens [46,47].

Equation (4) shows that larger the value of U , the shorter is τ_{on} , while the natural relaxation τ_{off} still plays an important role. The problem of large τ_{off} has been addressed in the past by using thinner cells or polymer-stabilized NLC. However, thinner cells result in a reduced OPD, and thus, small OP of the lens, while adding the polymer component causes increased light scattering that is also very undesired [48,49].

Here several possibilities to overcome this problem are proposed. One of them follows the example, reported in [50], that addresses the need for fast switching of the MTLCL by using the frequency dependence of the NLC material itself (in contrast with the above mentioned structural dependence). This is a family of materials that we actually already use that is called

dual-frequency NLC (DFNLC). It is well known that, in NLCs with positive dielectric anisotropy $\Delta\epsilon$, the director tends to be reoriented along the applied electric field, while in NLCs with negative dielectric anisotropy, the director is "repulsed" from the electric field (towards the perpendicular plane). In DFNLCs, the $\Delta\epsilon$ may change from a positive to a negative value with the change (increase) in the frequency of the applied electric field [26,51]. The frequency, at which such a change of sign occurs, is known as the crossover frequency f_c . This distinctive behavior of DFNLC allows for the better control of switching times of NLCs not only by maintaining a desired level of excitation voltage, but also by changing its frequency from low f to higher F values. The above-mentioned repulsion process, coupled with the original surface alignment, allows recovering the initial (ground state) alignment faster compared to the case of natural relaxation. Thus, to benefit from the DFNLC character of NLC mixtures, F and f values must be chosen to have them at opposite sides of the f_c (12 kHz for the DFNLC MLC-2048 used here).

To study the dynamic behavior of tunable lens (all measurements were performed at room temperature, $T = 292^\circ$ K), first, qualitative measurements of the wavefront of light transmitted through this lens were taken. A polarimetric imaging system was used for this purpose (see, e.g., [52,53] for details). Namely, the MTLCL (with a single NLC layer) was placed between two crossed polarizers with the ground state orientation of the director along the diagonal (at 45° between two crossed polarizers). Thus, the incident probe beam (obtained from the same CW He-Ne laser) generated both ordinary and extraordinary polarized waves inside the NLC. The second polarizer was used as an analyzer, which "projected" these two waves onto its transmission axis' direction to produce their interference. The ordinary wave experiences a uniform phase shift everywhere in the NLC layer, while the phase shift for the extraordinary wave is different depending upon the position with respect to the center of the lens. Thus, the above-mentioned interference will generate light fringes (see Fig. 6) the distances of which will be defined by the achieved phase shift (the distance between two dark fringes correspond to 2π shift on the wavefront) and thus will represent the evolution of the OP's value (the number of these rings can be used to estimate the value of the achieved OP [53], see hereafter for more quantitative details). These images were recorded by a camera in real time at the speed of 6 frame/s.

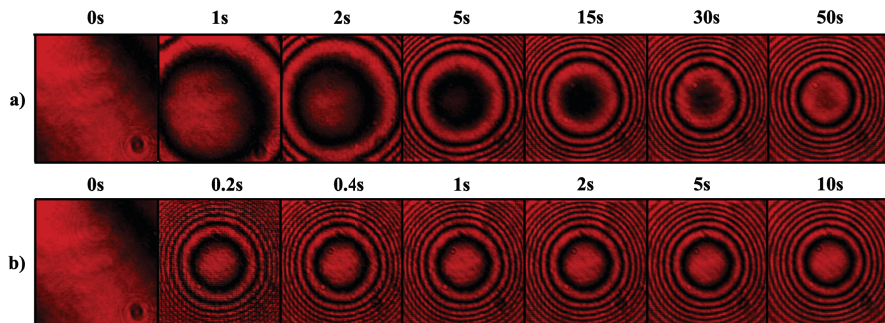


Fig. 6. Temporal evolution of polarimetric interference patterns (recording moments are displayed on the top of each image), a) without overdrive, $U = 3.5$ V b) with overdrive 20 V applied during $\Delta t = 0.19$ s.

Figure 6(a) shows a sequence of non-optimized excitation conditions. As we can see, initially (on the left, $t=0$ s) there are no fringes. The small variation of the brightness (along the diagonal) is related to the non uniformity of the NLC cell gap. Then, the direct application of excitation at 3.5 V generates a spherical wavefront delay and corresponding concentric fringes. It can be seen that the desired OP value is achieved very slowly (50 s). It is clear that such transition times are not acceptable.

To increase the transition speed, before the application of the final driving voltage $U_0 = 3.5$ V (corresponding to the desired value of OP), we can first apply a high-voltage *sin* wave U_h during a short time interval Δt (see Eq. (4)). Hereafter, we refer to this burst of *sin* waves as "overdrive" (OD) pulses. Figure 6(b) shows an example of a sequence of optimized excitation (with an OD, applied during $\Delta t = 0.19$ s). As one can see, in this case, the focusing lens is formed much faster (multiple rings already appear already in the second picture from the left).

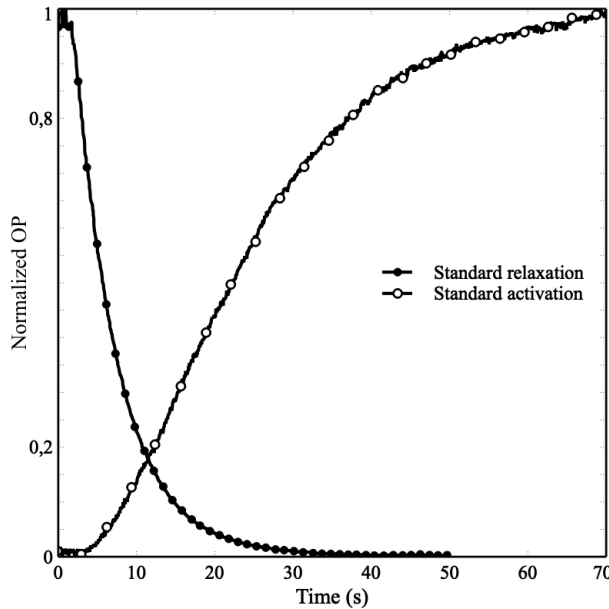


Fig. 7. Example of a non-optimized transition dynamics (change of the normalized optical power, OP) illustrating the slow response during the activation (turn-on) and relaxation for the following specific example of electrical excitation conditions : $U = 3.5$ V, $F = 120$ Hz, $U_{off} = 1.2$ V, and $f = 20$ Hz.

Next, the same SHWFS were used for more quantitative analyses of transition times. Here again, an example of a non optimized excitation condition is selected to demonstrate the importance of an accurate choice of driving parameters. The transition time is measured between the original (ground state; OP=0 D) quasi-planar uniform alignment (here named S_1) of the NLC and a predefined focusing state (named S_2) for the following excitation parameters: Amplitude and frequency of the high frequency signal $U = 3.5$ V, $F = 120$ Hz, and the parameters of the low frequency (offset signal) $U_{off} = 1.2$ V, $f = 20$ Hz. The "standard" experimental curves, shown in Fig. 7, correspond to this transition from S_1 to S_2 (non optimized activation) and from S_2 to S_1 (natural relaxation). The vertical axis shows the dynamic value of OP (normalized on the maximum OP), while the horizontal axis represents time (in seconds). These measurements were performed by using the same probe beam, a polarizer (aligned with the NLC's director to generate only extraordinary polarized light inside the NLC), the tunable lens, and a relay lens that was forming the image of the output plane of the proprietary lens on the SHWFS. The tunable lens was driven by *sin* wave voltages with modulated frequency and amplitude alternations (see the details in [24]). Voltage waveform generation, data acquisition, and analysis were performed in real time by using a proprietary (home-made) software.

In the next experiment, various OD conditions were used to optimize (reduce) the transition times. Figure 8 shows examples of optimized OD pulse amplitudes and durations Δt that allowed obtaining significantly better (shorter) rise times τ_{on} . For example, if we choose $\Delta t = 0.75$ s at 14

V , then τ_{on} becomes smaller (about 2.1 s). It is important to emphasize that the exaggeration of OD excitation level may also increase the time needed to reach the desired value of OP. Thus, as can be ascertained (e.g. in Fig. 8(a)), the $\Delta t = 0.9$ s duration of OD is excessive and the final (desired) value of OP is reached significantly later compared to the case with the same amplitude of OD excitation but maintained during $\Delta t = 0.8$ s.

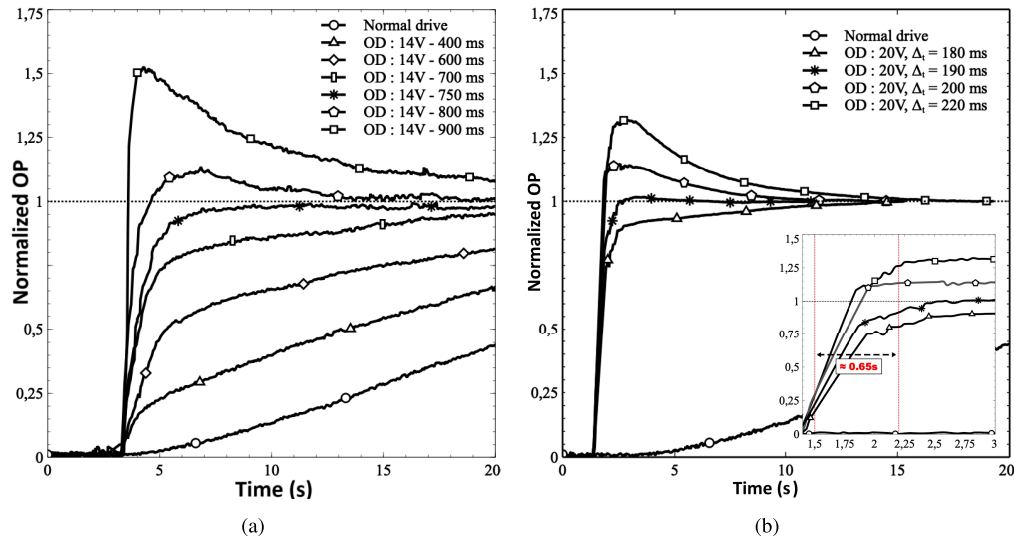


Fig. 8. Examples of optimization of the speed of the MTLCL with a) 14 V and b) 20 V overdrive (OD) voltages, applied with various pulse durations (Δ_t), compared with the normal drive response (without overdrive).

Furthermore, if it were decided to increase the amplitude of the overdrive pulse up to 20 V, for $\Delta t = 0.19$ s, then τ_{on} becomes even smaller (≈ 0.6 s, Fig. 8(b)). It is a clear improvement in comparison to the non-optimized approaches; e.g., when the final voltage is directly applied ($\Delta t = 0$) that provides a τ_{on} about 50 s.

There are other ways to accelerate transitions. For example, the non-focusing state ($OP = 0$ D) may be achieved not only in the ground state, but also when the cell is uniformly activated. Namely, a lens can be first generated in a specific "focusing" state (say S2). Then, the excitation can be removed, after which natural relaxation will occur (when the director is back to its ground state), or voltage can be applied with high frequency (above f_c) to force this back reorientation. In contrast, the excitation can be "continued" up to the saturation of the director's reorientation. That is, one can take advantage of the fact that at low excitation frequencies, the electrical potential U propagates well across the NLC cell (almost uniformly over the lateral dimension of the layer). Thus, high voltage can be applied with rather low-frequency excitation (e.g., $f = 120$ Hz) at which the used NLC has positive dielectric anisotropy (below f_c). As a result, the director may be uniformly reoriented towards the homeotropic state (S3) where the director is aligned along the applied electrical field everywhere in the cell. This state will have $OP = 0$ D, it may be reached very quickly and, in addition, it will demonstrate the lowest possible light scatter [31].

Subsequently, it is possible to return to the S2 state (with specific OP value) by changing the frequency of excitation or to go back to the initial planar alignment S1 either naturally or by applying a high-frequency voltage (using the negative sign of the dielectric anisotropy $\Delta\epsilon < 0$ when a frequency above f_c is used).

The corresponding demonstrations and measurements of the turn-off time were performed at frequencies of 30 kHz, 70 kHz and 120 kHz (above f_c). For this experiment, two different

amplitudes of driving signals were applied, $U = 6$ V and $U = 14$ V. A few examples of the obtained electro-optical response of the MTLCL are shown in Fig. 9.

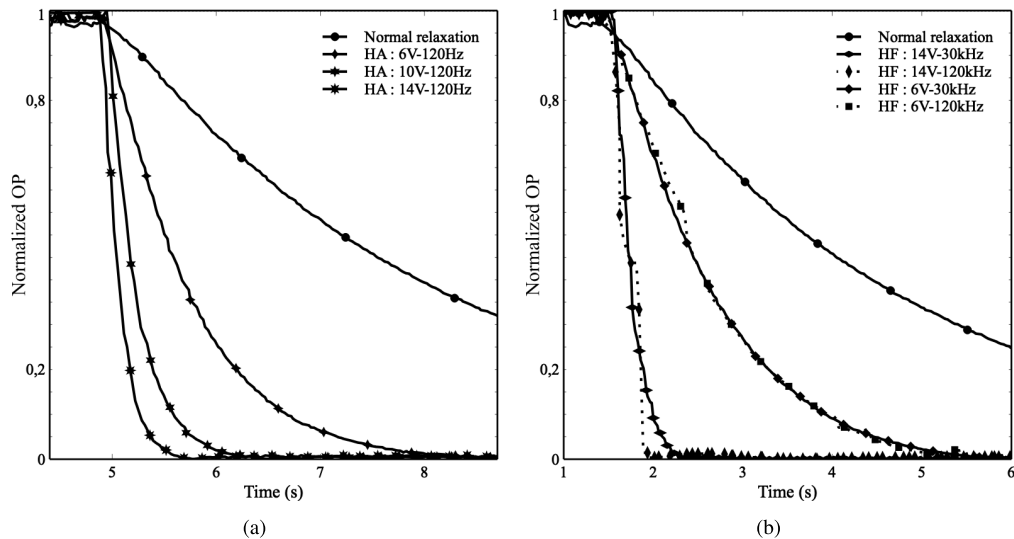


Fig. 9. Demonstrations of transition times with relatively high amplitude (HA) excitations at various frequencies from a predefined lens state (S2) to either a) to a quasi homeotropic state S3, or b) to a quasi planar state S1, both with zero OP.

Thus, according to Fig. 9 and Fig. 8, the turn-on time and turn-off times can be rather short (at the order of a half second), which makes DFNLC materials quite suitable for ophthalmic applications.

2.3. Application in presbyopia correction

Encouraged by the results obtained, the team proceeded to tests of human VA. The measurement of VA in the referenced studies is in agreement with the Logarithm of the Minimum Angle of Resolution (logMAR) chart methodology, closely aligning with the Early Treatment Diabetic Retinopathy Study (ETDRS) standard [54]. This procedure involves presenting participants with lines of five random letters, selected from "Sans Font Sloan" letters [55,56], with each subsequent line decreasing in size by 0.1 logMAR to incrementally assess the smallest detail the participant can accurately discern. The testing progresses until the participant incorrectly identifies three or more letters on the same line, at which point the acuity level of that line (adjusted by subtracting 0.02 logMAR for each letter incorrectly identified) is recorded as the participant's VA. This method provides a standardized way to evaluate visual performance under various conditions and with different visual corrections.

Approval for the study was obtained (study number 2021-272/23-09-2021) in accordance with the rules of the Comité d'éthique (ethics committee) de la recherche de l'Université Laval. Before the experimental procedures, informed consent was obtained from each patient after the nature of the study was explained. Exclusion criteria included myopia, ocular disease, amblyopia and/or strabismus and a history of ocular surgery or inflammation. Indeed, while the MTLCL may provide both positive and negative OP values (depending upon the LC and electrical control signals used), at this stage, all myopic patients were excluded (-0.5D and beyond) and the device developed was tested only for presbyopia correction. For this group of patients, no other requirements were specified, but the maximal OP was limited to +3 D (the local lens' OP was varied from 0 to +3.00 D on the defocus in steps of 0.5 D).

The study comprised three phases. First, the eye prescriptions of the patients were analysed; second, their VAs were evaluated; and third, attempts were made to correct their eyes' aberrations (defocus and astigmatism). The "wearer" of the MTLCL looked at charts at different distances, repeated once with no correction and once with the MTLCL being activated for correction. The next step was to find a local maximum of perceived visual quality by electrically tuning the lens properties (correction order was alternated between participants).

The proof of concept test was carried out on 7 subjects (aged between 45 to 70 years old), who were already examined by an ophthalmologist. Thus, the exact eye prescriptions were already known on the basis of the corresponding prescription.

The correction procedure chosen was non-contact and without prior manipulation. MTLCL replaced the user's correction (pair of eyeglasses). The patient's head was positioned with temple supports and a chin rest to observe the scene presented in Fig. 5(a), which no longer included targets for estimating the MTF, but instead featured EDTRS targets for VA testing. Three targets were positioned at 35cm, three others at 1 meter; targets at 2.8 meters were placed within the field of view in the back of the scene. Letter sizes (in these targets) were adjusted according to the distances, with a print resolution of 300 dots per inch (dpi). At a given distance, multiple targets were analyzed within the total FoV. To minimize memory effects, the target was replaced with each increment of the lens's OP. For a given distance, the VA for each target was averaged to determine the corresponding VA.

While an eye was analyzed, an eye-patch was placed in front of the second eye. Scene illumination was set to approximately 50 cd/m² to ensure comfort due to the sensitivity of the retina (with two white LEDs of 6200 Kelvin, with diffusors for homogenization).

The MTLCL logMAR VA (defocus curve; range from 0 to +3.00 D in 0.50 D steps) was evaluated.

It is worth reminding that the eyeglass prescription consists of spherical power *Sphere*, cylindrical power *Cyl* related to the astigmatism value, an axis direction, *axis* and additional magnifying power needed for near work, *ADD* diagnosis. They can be computed (see hereafter for definitions) from the Zernike amplitudes [57]:

$$\begin{aligned} Cyl &= 2\sqrt{J_o^2 + J_{45}^2}, \\ \text{Sphere} &= D_r - \frac{Cyl}{2}, \\ \text{axis} &= -\arctan\left(\frac{Cyl/2 + J_0}{J_{45}}\right) \end{aligned} \quad (5)$$

Using the coefficients measured by the SHWFS, it is possible to convert these values into diopters, which quantify the OP of lenses. First-order Zernike polynomials, as defocus and astigmatism, may be represented by mathematical expressions of a concave or convex wavefront [57]. The Peak Valley (PV) value, which represents the wavefront deviation is independent of the physical diameter of the pupil, as it solely describes the wavefront deviation along the Z-axis. To convert the PV value into the radius of curvature (RoC), a standard circle function was employed based on the "sagitta" formula [58]. After calculating the RoC, this value was converted to diopters (1/RoC), with D_r , the defocus diopter, J_0 et J_{45} the 90/180 and oblique astigmatisms, respectively. The following equations were obtained [59]:

$$D_r = \frac{-16\sqrt{3}.a_4}{d^2}, \quad J_0 = \frac{-8\sqrt{6}.a_5}{d^2}, \quad J_{45} = \frac{-8\sqrt{6}.a_6}{d^2} \quad (6)$$

Where d is the pupil size; a_4 , a_5 and a_6 are the Zernike coefficients for defocus and astigmatism, respectively. These equations show that the MTLCL is able to tune diopter correction with a precise control of Zernike coefficients [25].

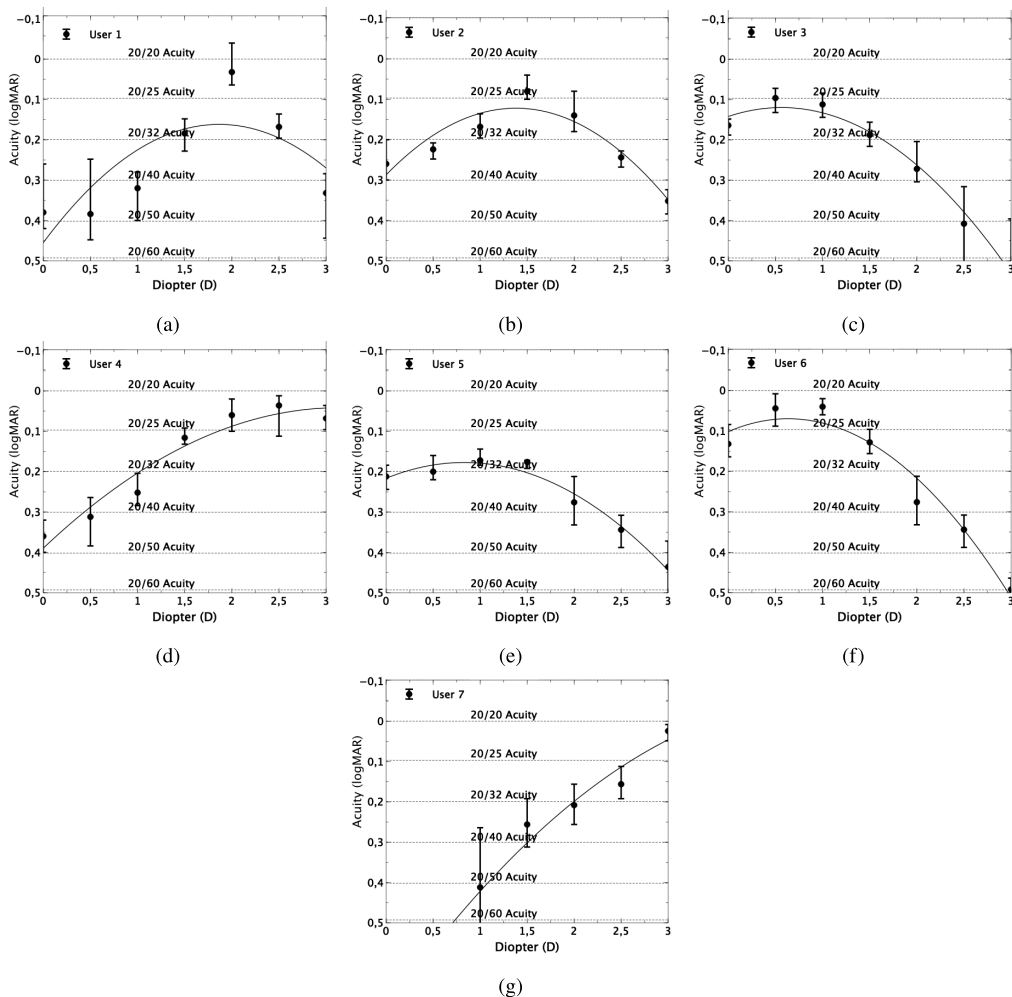


Fig. 10. Demonstration of the impact of the MTLCL on visual acuity of 7 patients (the targets were placed at 35 cm).

Coming back to the tests performed, a specific example of the applied procedure is as follows : the target was placed at 35 cm, refractive error ranged from +0.50 to +3.75 D (median spherical equivalent, +1.65 D). Astigmatism values for examined patients ranged from 0 to 1.25 D (median, 0.42 D), with the optimum correction acuity ranging from -0.04 to +0.18 logMAR. No preliminary corrections (sphere or cylinder) were applied before the additional power was applied for the presbyopic correction. Figure 10 presents the measured impact (individualized for each 7 patients) of the MTLCL's tuning on their VA, showcasing both the overall enhancement and the variation in performance across different patients. It can be seen that the obtained VA is a little lower than desired in most cases. There may be several reasons for this. First, at present, experiments were carried out without an eye tracking system. The transversal positions of local lenses (to be activated) were pre-registered to align (approximately) the retina, lenses and corresponding targets (in fixed positions). Better positioning of each lens (e.g., by using an eye tracking system to follow the movements of the head and thus of the eye) should enable better alignment and results. Also, the printing quality of the targets used was not very good. Indeed, the targets were printed with 300 dpi resolution (in theory it should be sufficient for printing

letters corresponding to 20/20 at 35 cm). However, it would have been preferable to print in 600 dpi to reduce (as much as possible) the degradation of edges on small letters, which can impact on the reading quality.

The comparison of average VA for users is presented in Fig. 11 in comparison between natural vision refers to the participants' unaided vision (i.e., no glasses or MTLCL) and when the MTLCL lens is activated and optimized (voltages and position) in the first approximation to the best perceived VA. As can be seen, here again, a rather significant improvement is obtained, by a factor of 3.4. The final state is very close to 20/20 vision.

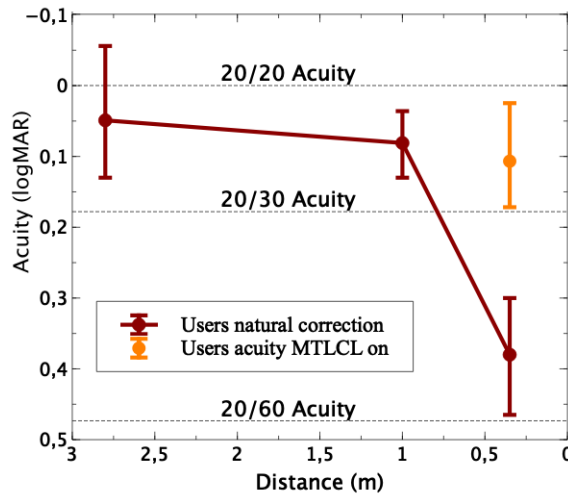


Fig. 11. Comparison between natural correction and when the MTLCL lens is activated (by using the average VA for users). The error bars represent the variation of VA across participants at best accommodation state.

3. Discussion and conclusion

As already mentioned, other physical mechanisms have been considered in the past to dynamically correct presbyopia. However, the reported (in the scientific literature) work with human tests seems to be very limited. For example, Monpean et al., report the use of a couple of liquid lenses (driven by pupil tracking) to correct presbyopia [60]. However, in addition to the presence of mechanical deformation (inside the structure of the lens), such lenses usually require very high voltages (up to 140V, [9]) and consequently their electrical power consumption will be very high.

That is why, it seems that the lens introduced here represents high potential for ophthalmic (mobile) applications. Already preliminary experimental tests conducted with a small group of patients have demonstrated that this lens effectively corrects the vision almost to natural vision, suggesting its potential as a practical solution for presbyopia correction. In addition, the same device can be used to dynamically generate various types of wavefront deformations (coma, astigmatism, etc., [25]) to correct corresponding aberrations in the human eye.

One of the performance aspects is the reaction speed. Its optimization (0.5 sec) was done at room temperature. At the same time, it is well known that LCs react differently for different temperatures (slower for low temperatures). For higher temperatures, the performance of the lens will be faster, but the OP of the lens will degrade if the temperature is close to the so-called nematic-isotropic phase transition temperature T_c . However, currently, LC mixtures are available that have a $T_c = 145^\circ\text{C}$. Thus, if the lens is used well below these temperatures (say, below 100°C), then the variations of the temperature will not noticeably affect the focusing capability.

Concerning the overall performance : as already mentioned, an eye-tracking system must be added to the device to provide information about the direction (to define the appropriate position of the local lens to be activated) as well as the distance (to define the value of OP to be generated) of the object of interest. Such devices are already widely used in Virtual Reality headsets and other mobile devices (displays, etc.), see, e.g., [61]. Most of them use either a camera or an emitter coupled with an array of photo detectors to track the eye direction and the distance of objects of interest. They are very miniature and will not add much volume and weight. In contrast, their integration will provide a more natural visual correction method that aligns closely with the physiological processes ongoing in the human eye.

The currently used substrates are thick (0.55 mm) for the easy manipulation of the prototype. However, the final (portable) device may be produced by using the latest generation of LC display manufacturing procedures to make it very thin. The best procedure known today uses 0.1 mm thick glass substrates (the 0.2 mm is already well mastered). This means that the total thickness of the element under discussion may be reduced down to 0.54 mm. The authors believe that this would be quite acceptable as thickness (standard eye glasses may be 3 mm thick in the center and 4 mm thick at the periphery).

While the current study focuses only on the ophthalmic case, it is worth mentioning that this capability of simultaneous focusing and wavefront tilting, provided by the proposed device, might be also explored to solve the vergence accommodation problem in virtual reality applications [62].

In addition, it was already demonstrated [25] that one can use the same device to generate also negative lenses, which may offer promising avenues for the simultaneous presbyopia and myopia corrections by the same device. Interestingly enough, this may be achieved by using dual frequency NLCs, which, in addition, may also help to further decrease the response time of the device developed.

Obviously, further developments and experiments must be conducted to explore the full potential of the proposed approach, including the lens (for example, the reported here tests were limited to the FoV of the camera used, while the lens has the potential for wide FoV operation) and the eye tracking integration aspects. In the case of success (integration and operation), such a solution may help millions of people worldwide. The study reported here is only the first step, but it already showcases the technical feasibility of the device and sets the stage for its further development and integration into a practical and user-friendly device.

Funding. Natural Sciences and Engineering Research Council of Canada (05888); Canada Research Chairs (230212).

Acknowledgments. We would like to thank LensVector inc and PATQER Photonique inc for their material support.

Disclosures. Authors have no conflict of interest to disclose.

Data availability. Additional information may be obtained by contacting the authors.

References

1. A. Glasser and M. C. Campbell, "Presbyopia and the optical changes in the human crystalline lens with age," *Vision Res.* **38**(2), 209–229 (1998).
2. A. Glasser and M. C. Campbell, "Biometric, optical and physical changes in the isolated human crystalline lens with age in relation to presbyopia," *Vision Res.* **39**(11), 1991–2015 (1999).
3. A. Duane, "Studies in monocular and binocular accommodation with their clinical applications," *Am. J. Ophthalmol.* **5**(11), 865–877 (1922).
4. B. A. Holden, T. R. Fricke, S. M. Ho, *et al.*, "Global vision impairment due to uncorrected presbyopia," *Arch. Ophthalmol.* **126**(12), 1731–1739 (2008).
5. C. W. Brooks, *System for Ophthalmic Dispensing-E-book* (Elsevier Health Sciences, 2023).
6. J. E. Sheedy, C. Campbell, E. King-Smith, *et al.*, "Progressive powered lenses: the minkwitz theorem," *Optom. Vis. Sci.* **82**(10), 916–922 (2005).
7. W. N. Charman, "Developments in the correction of presbyopia ii: surgical approaches," *Ophthalmic Physiol. Opt.* **34**(4), 397–426 (2014).
8. L. W. Alvarez, "Two-element variable-power spherical lens," (1967). US Patent 3,305,294.

9. J. Jarosz, N. Molliex, G. Chenon, *et al.*, "Adaptive eyeglasses for presbyopia correction: an original variable-focus technology," *Opt. Express* **27**(8), 10533–10552 (2019).
10. J. E. Floyd, "Fluid filled and pressurized lens with flexible optical boundary having variable focal length," (1997). US Patent 5,684,637.
11. S. Kuiper and B. H. W. Hendriks, "Variable focus spectacles," (2009). US Patent 7,553,019.
12. Y.-H. Lin and H.-S. Chen, "Electrically tunable-focusing and polarizer-free liquid crystal lenses for ophthalmic applications," *Opt. Express* **21**(8), 9428–9436 (2013).
13. H.-S. Chen, M.-S. Chen, and Y.-H. Lin, "Electrically tunable ophthalmic lenses for myopia and presbyopia using liquid crystals," *Mol. Cryst. Liq. Cryst.* **596**(1), 88–96 (2014).
14. J. Bailey, P. B. Morgan, H. F. Gleeson, *et al.*, "Switchable liquid crystal contact lenses for the correction of presbyopia," *Crystals* **8**(1), 29 (2018).
15. T. Galstian, K. Asatryan, V. Presniakov, *et al.*, "Electrically variable liquid crystal lenses for ophthalmic distance accommodation," *Opt. Express* **27**(13), 18803–18817 (2019).
16. S. P. Kern, "Variable power lens system," (1986). US Patent 4,601,545.
17. P. Valley, M. Reza Dodge, J. Schwiegerling, *et al.*, "Nonmechanical bifocal zoom telescope," *Opt. Lett.* **35**(15), 2582–2584 (2010).
18. W. Feng and M. Ye, "Refractive fresnel liquid crystal lenses driven by two voltages," *Opt. Express* **32**(1), 662–676 (2024).
19. A. Pusenkova, O. Sova, and T. Galstian, "Electrically variable liquid crystal lens with spiral electrode," *Opt. Commun.* **508**, 127783 (2022).
20. O. Sova and T. Galstian, "Modal control refractive Fresnel lens with uniform liquid crystal layer," *Opt. Commun.* **474**, 126056 (2020).
21. A. Jamali, D. Bryant, Y. Zhang, *et al.*, "Design of a large aperture tunable refractive fresnel liquid crystal lens," *Appl. Opt.* **57**(7), B10–B19 (2018).
22. O. Sova, V. Presniakov, A. Zohrabyan, *et al.*, "Large diameter electrically tunable lens for ophthalmic distance accommodation," *Biomed. Opt. Express* **14**(12), 6317–6327 (2023).
23. T. Galstian, "Electrode structure for foveal lens device," U.S. Provisional Patent Application 63/211,396 (2021).
24. L. Bégel, B. Khodadad, and T. Galstian, "Adaptive lens for foveal vision, imaging, and projection over large clear apertures," *Opt. Express* **31**(2), 2877–2891 (2023).
25. B. Louis and G. Tigran, "Dynamic control of defocus, astigmatism, and tilt aberrations with a large area foveal liquid crystal lens," *Appl. Opt.* **63**(11), 2798–2805 (2024).
26. A. B. Golovin, S. V. Shiyanskii, and O. D. Lavrentovich, "Fast switching dual-frequency liquid crystal optical retarder, driven by an amplitude and frequency modulated voltage," *Appl. Phys. Lett.* **83**(19), 3864–3866 (2003).
27. Y.-Y. Kao and P. C.-P. Chao, "A new dual-frequency liquid crystal lens with ring-and-pie electrodes and a driving scheme to prevent declination lines and improve recovery time," *Sensors* **11**(5), 5402–5415 (2011).
28. J. Stevens and T. Galstian, "Electrically tunable liquid crystal lens with a serpentine electrode design," *Opt. Lett.* **47**(4), 910–912 (2022).
29. M. Ye, B. Wang, and S. Sato, "Double-layer liquid crystal lens," *Jpn. J. Appl. Phys.* **43**(No. 3A), L352–L354 (2004).
30. A. Bagramyan and T. Galstian, "Dynamic control of polarization mismatch and coma aberrations in rod-grin assemblies," *Opt. Express* **27**(10), 14144–14151 (2019).
31. T. Galstian, O. Sova, K. Asatryan, *et al.*, "Optical camera with liquid crystal autofocus lens," *Opt. Express* **25**(24), 29945–29964 (2017).
32. C. A. Curcio, K. R. Sloan, R. E. Kalina, *et al.*, "Human photoreceptor topography," *J. Comp. Neurol.* **292**(4), 497–523 (1990).
33. A. Jackson and I. Bailey, "Visual acuity," *Optometry in Practice* **5**, 53–68 (2004).
34. G. A. Osterberg, "Topography of the layer of rods and cones in the human retina," *Acta Ophthalmol.* **108**, 232 (1935).
35. C. A. Curcio, K. R. Sloan Jr, O. Packer, *et al.*, "Distribution of cones in human and monkey retina: individual variability and radial asymmetry," *Science* **236**(4801), 579–582 (1987).
36. W. J. Smith, *Modern Optical Engineering: The Design of Optical Systems* (McGraw-Hill Education, 2008).
37. Y. Wu, C. P. Chen, L. Mi, *et al.*, "Design of retinal-projection-based near-eye display with contact lens," *Opt. Express* **26**(9), 11553–11567 (2018).
38. R. Navarro, "The optical design of the human eye: a critical review," *J. Optom.* **2**(1), 3–18 (2009).
39. P. Zhao, C. Ataman, and H. Zappe, "Spherical aberration free liquid-filled tunable lens with variable thickness membrane," *Opt. Express* **23**(16), 21264–21278 (2015).
40. L. Sun, S. Sheng, W. Meng, *et al.*, "Design of spherical aberration free liquid-filled cylindrical zoom lenses over a wide focal length range based on zemax," *Opt. Express* **28**(5), 6806–6819 (2020).
41. J. A. Mordini and K. J. Ciuffreda, "Dynamic aspects of accommodation: age and presbyopia," *Vision Res.* **44**(6), 591–601 (2004).
42. Y.-H. Lin, Y.-J. Wang, and V. Reshetnyak, "Liquid crystal lenses with tunable focal length," *Liq. Cryst. Rev.* **5**(2), 111–143 (2017).
43. P.-G. De Gennes and J. Prost, *The physics of liquid crystals*, 83 (Oxford university press, 1993).
44. X. Nie, R. Lu, H. Xianyu, *et al.*, "Anchoring energy and cell gap effects on liquid crystal response time," *J. Appl. Phys.* **101**(10), 103110 (2007).

45. L. M. Blinov and V. G. Chigrinov, *Electrooptic Effects in Liquid Crystal Materials* (Springer Science & Business Media, 2012).
46. M. Loktev, "Modal wavefront correctors based on nematic liquid crystals," Ph. D. dissertation (2005).
47. L. Tabourin, D. Brousseau, S. Thibault, *et al.*, "Wavefront control capability in a modal lens with segmented circular peripheral electrodes," *Appl. Opt.* **62**(30), 7970–7976 (2023).
48. A. Pusenkova and T. Galstian, "Reducing the light scattering impact in liquid-crystal-based imaging systems," *Appl. Opt.* **59**(16), 4780–4789 (2020).
49. Y.-H. Lin, W.-C. Cheng, H.-S. Chen, *et al.*, "Orientation fluctuation in liquid crystal lenses," *J. Opt. Microsystems* **3**(04), 041204 (2023).
50. O. Pishnyak, S. Sato, and O. D. Lavrentovich, "Electrically tunable lens based on a dual-frequency nematic liquid crystal," *Appl. Opt.* **45**(19), 4576–4582 (2006).
51. H. Xianyu, S.-T. Wu, and C.-L. Lin, "Dual frequency liquid crystals : a review," *Liq. Cryst.* **36**(6-7), 717–726 (2009).
52. L. Tabourin and T. Galstian, "Liquid crystal module for motionless generation of variable structured illumination," *J. Opt. Soc. Am. B* **37**(7), 2064–2070 (2020).
53. L. Begel and T. Galstian, "Liquid crystal lens with corrected wavefront asymmetry," *Appl. Opt.* **57**(18), 5072–5078 (2018).
54. F. L. Ferris III, A. Kassoff, G. H. Bresnick, *et al.*, "New visual acuity charts for clinical research," *Am. J. Ophthalmol.* **94**(1), 91–96 (1982).
55. I. L. Bailey and J. E. Lovie, "New design principles for visual acuity letter charts," *Optom. Vis. Sci.* **53**(11), 740–745 (1976).
56. J. T. Holladay, "Proper method for calculating average visual acuity," *J. Refract. Surg.* **13**(4), 388–391 (1997).
57. V. Lakshminarayanan and A. Fleck, "Zernike polynomials: a guide," *J. Mod. Opt.* **58**(7), 545–561 (2011).
58. Wikipedia, "Sagitta (geometry)," (2024).
59. X. Cheng, A. Bradley, S. Ravikumar, *et al.*, "Visual impact of Zernike and Seidel forms of monochromatic aberrations," *Optom. Vis. Sci.* **87**(5), 300–312 (2010).
60. J. Mompeán, J. L. Aragón, and P. Artal, "Portable device for presbyopia correction with optoelectronic lenses driven by pupil response," *Sci. Rep.* **10**(1), 20293 (2020).
61. H. Singh and J. Singh, "Human eye tracking and related issues: A review," *International Journal of Scientific and Research Publications* **2**, 1–9 (2012).
62. Y. Zhou, J. Zhang, and F. Fang, "Vergence-accommodation conflict in optical see-through display: Review and prospect," *Results Opt.* **5**, 100160 (2021).